AMP in the circadian pacemaking system at the biochemical level should aid in the search for the molecular components of the oscillator.

ARNOLD ESKIN

Department of Biology,
University of Houston,
Houston, Texas 77004

JOSEPH S. TAKAHASHI

Section on Pharmacology,
Laboratory of Clinical Science,
National Institutes of Mental Health,
Bethesda, Maryland 20205

References and Notes

1. J. S. Takahashi and M. Zatz, *Science* **217**, 1104 (1982).
2. A. Eskin, *Fed. Proc. Fed. Am. Soc. Exp. Biol.* **38**, 2573 (1979).
3. G. Corrent and A. Eskin, *Am. J. Physiol.* **242**, R333 (1982).
4. G. Corrent, D. J. McAdoo, A. Eskin, *Science* **202**, 977 (1978).
5. *Aplysia californica* specimens were maintained in artificial seawater at 15°C and entrained to a light-dark cycle (LD) of 12 hours of light and 12 of darkness. Eyes were dissected at the end of the light period and maintained at 15°C in the dark for 3 to 4 hours before they were frozen on dry ice. Frozen eyes from 9 to 15 animals were homogenized in ice-cold buffer containing 10 m*M* tris-HCl (*p*H 7.6), 5 m*M* $MgCl_2$, 1 m*M* dithiothreitol, and 1 m*M* EGTA (25 μl of buffer per eye). Enzyme activity was assayed in a 50-μl reaction mixture containing (final concentrations) 42 m*M* tris-HCl (*p*H 8.0), 6 m*M* $MgCl_2$, 0.7 m*M* EGTA, 0.5 m*M* isobutylmethylxanthine, 0.2 m*M* dithiothreitol, 1 m*M* adenosine triphosphate (ATP), 5 to 25 μg of protein (10 μl of homogenate), and drug as indicated. Reactions were initiated by addition of ATP and incubated for 20 minutes at 30°C. Reactions were stopped by adding 250 μl of 50 m*M* sodium acetate buffer, *p*H 6.5, and boiling for 3 minutes. Cyclic AMP formed was measured by radioimmunoassay [A. L. Steiner, C. W. Parker, D. M. Kipins, *J. Biol. Chem.* **247**, 1106 (1972)] with components from Becton Dickinson Immunodiagnostics. Under the conditions used, enzyme activity was proportional to time and to enzyme concentration. Protein was determined by the method of Lowry [O. H. Lowry, N. J. Rosebrough, A. L. Farr, R. J. Randall, *J. Biol. Chem.* **193**, 265 (1951)].
6. Basal adenylate cyclase activity varied between 0.6 and 3.1 pmoles of cyclic AMP per minute per milligram of protein. The activity of adenylate cyclase relative to basal levels (with basal = 100 ± 12 percent, mean ± standard error, $N = 4$) was: serotonin, 211 percent; dopamine, 90 percent; octopamine, 115 percent; and histamine, 103 percent [neurotransmitters were added at $10^{-5}M$; all tests contained $10^{-5}M$ guanosine triphosphate (GTP)]. Because the lens of the eye contains about 80 percent of the total protein, the specific activity of adenylate cyclase for retinal protein is five times higher than the values reported here. The serotonin stimulation of adenylate cyclase activity was potentiated by $10^{-5}M$ GTP. Sodium fluoride (10 m*M*) increased activity 14 times that of basal.
7. A. Eskin, G. Corrent, C.-Y. Lin, D. J. McAdoo, *Proc. Natl. Acad. Sci. U.S.A.* **79**, 660 (1982).
8. J. L. Luborsky-Moore and J. W. Jacklet, *J. Histochem. Cytochem.* **24**, 1150 (1976).
9. D. Weinreich, *Nature (London)* **267**, 854 (1977).
10. A. Eskin, *J. Neurobiol.* **8**, 273 (1977).
11. K. B. Seamon and J. W. Daly, *J. Cyclic Nucleotide Res.* **7**, 201 (1981).
12. Phosphodiesterase activity (in nanomoles of cyclic AMP per minute per milligram of protein) was: basal, 1.65; $10^{-5}M$ serotonin, 1.58; and $10^{-5}M$ forskolin, 1.56. Phosphodiesterase activity was assayed by a two-step procedure [W. J. Thompson *et al.*, *Adv. Cyclic Nucelotide Res.* **10**, 69 (1979)]. The final reaction mixture contained 41 m*M* tris-HCl (*p*H 8.0), 5.5 m*M* $MgCl_2$, 0.1 m*M* EGTA, 0.1 m*M* dithiothreitol, 100 μ*M* cyclic AMP, 1 μCi of cyclic [2,8-^{3}H]AMP (New England Nuclear), and 25 μg of protein (10 μl of homogenate) in a total volume of 100 μl. Reactions were incubated at 30°C for 20 minutes. Guanylate cyclase activity [in picomoles of cyclic guanosine monophosphate (GMP) per minute per milligram of protein] was: basal, 1.50; $10^{-5}M$ serotonin, 1.36; and $10^{-5}M$ forskolin, 1.22. Guanylate cyclase activity was tested under the same conditions as those used for adenylate cyclase with the exception that 1 m*M* GTP was substituted for the ATP. Cyclic GMP formed was tested by radioimmunoassay (Becton Dickinson Immunodiagnostics) [A. L. Steiner, C. W. Parker, D. M. Kipnis, *J. Biol. Chem.* **247**, 1106 (1972)].
13. G. Corrent, A. Eskin, I. Kay *Am. J. Physiol.* **242**, R326 (1982).
14. E. W. Sutherland and G. A. Robison, *Pharmacol. Rev.* **18**, 145 (1966).
15. Although inhibitors of protein synthesis have been shown to elicit phase shifts or changes in the period of circadian oscillators, the specific proteins involved in these effects have not been identified. Also, it is not clear what role the affected proteins play in these circadian systems [see J. W. Jacklet, *Biol. Bull. (Woods Hole, Mass.)* **160**, 199 (1981)].
16. We thank M. Zatz for helpful comments, B. Holcomb for editorial assistance, and S. C. Yeung for technical assistance. Supported in part by NSF grant BNS-792 4133. J.S.T. is a Pharmacology Research Associate of the National Institute of General Medical Sciences.

19 July 1982; revised 29 October 1982

Bidirectional Transmission at the Rectifying Electrotonic Synapse: A Voltage-Dependent Process

Abstract. *Rectifying properties of electrotonic synapses established by the crayfish giant motor fiber are associated with a more negative resting membrane potential in the presynaptic than in the postsynaptic side of the junction. An increased junctional conductance and bidirectional transmission are produced, with almost no delay, by inverting this polarization.*

Although electrotonic transmission through gap junctions is generally bidirectional (*1, 2*), in a few systems, the junctional resistance between coupled cells varies in such a way that currents flow more readily in one direction. In the crayfish giant motor synapse (GMS), spikes and passive depolarizations pass from the presynaptic lateral and medial giant axons to the postsynaptic giant motor fiber, whereas only hyperpolarizations spread in the opposite direction (*3, 4*). This property can be functionally significant (*4, 5*), but its origin remains

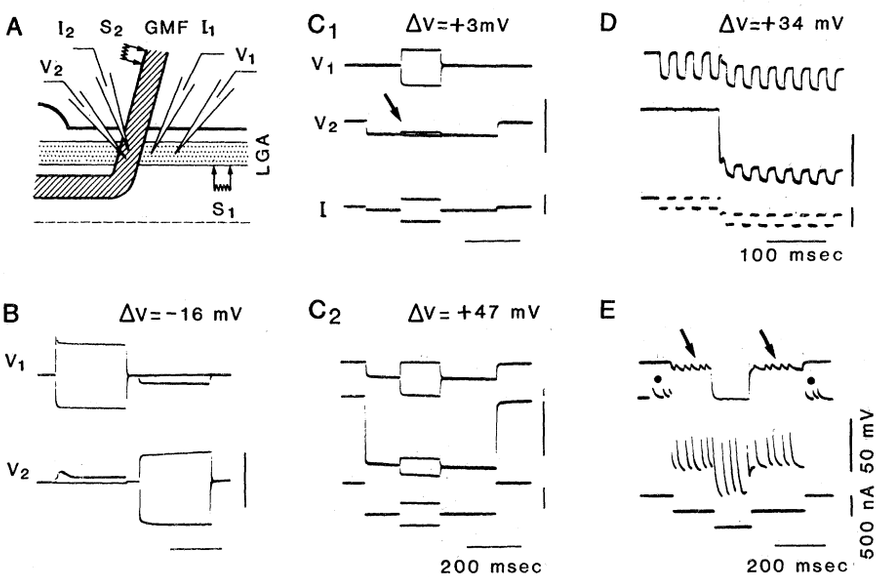

Fig. 1. Tests for the transmission of electrotonic potentials. (A) Diagram illustrating the microelectrodes (one for current passing, *I*, and one for voltage recording, *V*) inserted in the lateral giant axon (*LGA*, I_1, and V_1) and the giant motor fiber (*GMF*, I_2, and V_2) and the extracellular electrodes (S_1 and S_2). (B) Rectified transmission in resting conditions. (C to E) Voltage dependence of the rectification. Upper and middle traces: voltage recorded from presynaptic (V_1) and postsynaptic (V_2) cells; lower trace: superimposed current steps applied to pre- and postsynaptic sides of the junction. (C_1) During slight hyperpolarizations of the motor fiber, only positive pulses spread from the pre- to the postsynaptic side (arrow), with a calculated coupling coefficient *k* of about 0.16 (C_2). With stronger hyperpolarizations, synaptic transmission became bidirectional, *k* reaching 0.48 and 0.52 for positive and negative pulses, respectively. (D) Short negative pulses (25 msec) were applied to the presynaptic axon, and transynaptic spread of current began almost instantaneously with the onset of postsynaptic hyperpolarization. (E) Postsynaptic potentials occurring in the motor fiber (dots, middle traces) spread in the presynaptic axon (upper trace, arrows) during hyperpolarizations of the postsynaptic fiber moving ΔV from −17 to +53 mV. (A reduction of this potential difference by a short polarization of the lateral axon reversibly blocked the transynaptic effect, despite a concomitant increase in the amplitude of the postsynaptic potential.)

unclear, particularly since morphological investigations indicate that the axons are joined by gap junctions structurally similar to those of the nonrectifying septate synapses (*6*).

Furshpan and Potter (*4*) established that the junction behaves as a simple diode, "the intensity of the passive current flow across it depending only on the potential difference across the rectifier." Theirs was (to our knowledge) the first report of a voltage-dependent electrotonic synapse, albeit different from those studied later (*7*). In view of the additional evidence that at the GMS and adjacent rectifying synapses the resting membrane potentials of the pre- and postsynaptic cells differ significantly, we have reexamined the relations between transjunctional polarization and conductances. Direct evidence was obtained that in these models transmission can become bidirectional and junctional conductances can be markedly increased.

We dissected out the abdominal nerve cord of the crayfish *Procambarus* at the level of the third roots and continuously perfused with a Van Harreveld solution (*8*). Two microelectrodes filled with 3*M* KCl were inserted on each side of the GMS (Fig. 1A), and orthodromic or antidromic activations by means of bipolar electrodes further helped to identify the motor fiber. Short polarizing pulses were applied in one element in order to calculate coupling parameters from classical equations (*1, 9*), and longer pulses (about 500 msec long) were injected in the other side to modify, when required, the difference between the membrane potentials of the presynaptic cell (V_1) and the postsynaptic axon (V_2). The parameter $\Delta V = V_1 - V_2$ was calculated before injections of the short test pulses; that is, for each cell V was the sum of its own resting potential and the voltage modifications introduced by the polarizing currents, if any. Positive values of ΔV indicate that the presynaptic side of the junction was more positive than the postsynaptic fiber.

The rectifying properties of the GMS are illustrated in Fig. 1B. In this preparation, the membrane potentials of the pre- and postsynaptic axons were −91 and −75 mV, respectively; hence ΔV was −16 mV, which is within the characteristic range: its mean value and standard deviation were -14.6 ± 7.5 mV (N = 12), respectively [similar low values were reported in the motor fiber and its soma (*10*)].

As the giant motor fiber was made more negative, electrotonic spread of currents across the junction was first enhanced for positive presynaptic injections, and at values of ΔV averaging +15 mV (standard deviation = 5, N = 22), hyperpolarizing current steps began to spread transynaptically. For instance, in Fig. 1, C_1 and C_2, the transjunctional voltage evoked at rest by weak (220 nA) test currents was zero (not shown). With slight increases of ΔV, small depolarizations were recorded in the postsynaptic fiber (Fig. $1C_1$), and finally currents of either sign were transmitted symmetrically (Fig. $1C_2$). These modifications of transmission across the GMS ceased when the polarizing current was discontinued.

An important property of this voltage dependence was its rapid onset. The increase of the coupling ratio was already maximal at the earlier phase of the postsynaptic hyperpolarization (Fig. 1D), that is, immediately after the stimulus artifact, and it remained invariant throughout the polarizing step. Also, when the junctional polarization was appropriate, the GMS became capable of conducting antidromically synaptic potentials such as depolarizing inhibitory postsynaptic potentials, which occur spontaneously in the motor fiber (Fig. 1E) (*11*).

The conditions in which the GMS behaves as a symmetrical junction are summarized in Fig. 2A, which shows that the junctional resistance constitutes a voltage-sensitive element. Further experiments confirmed this view. In Fig. 2B, voltage transfer functions are plotted for different transjunctional voltages. While the spread of depolarizations increased as soon as ΔV was shifted from −11 to −1 mV, larger junctional polarizations were required for transmission of hyperpolarizing pulses. The transition from an asymmetrical junction to a bidirectional one was directly related to the junctional polarity. The calculated coupling coefficients k increased along near sigmoid curves until they reached (with a shift to the right for negative pulses) a steady-state plateau (Fig. 2C). This enhanced coupling was ascribable to a reduction of the junctional resistance R_J (Fig. 2D), which reached its minimal value (90 kilohm in this case) when ΔV approximated

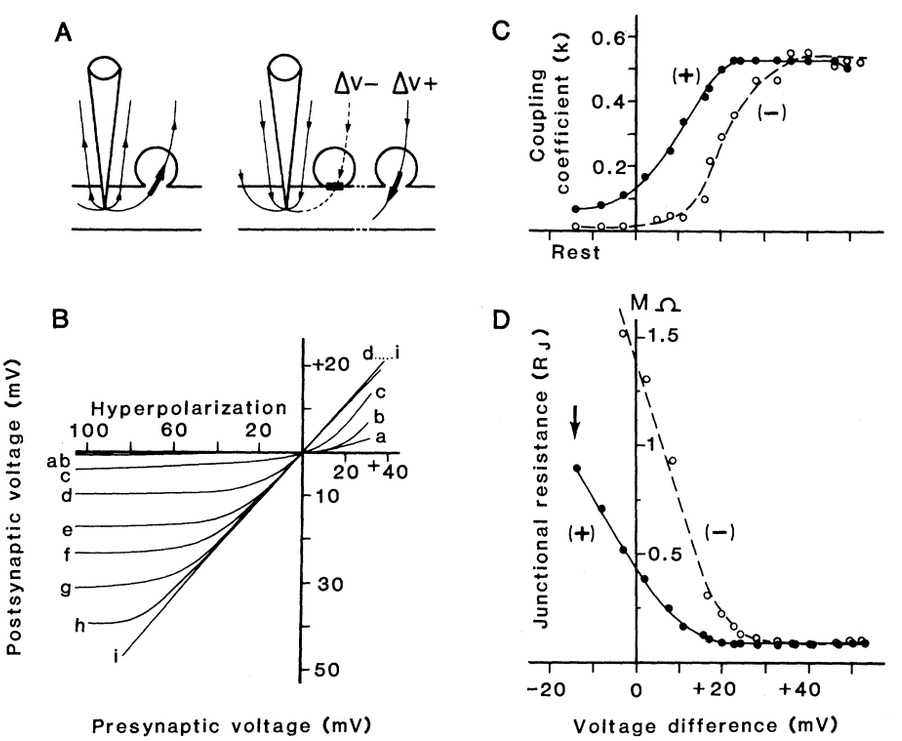

Fig. 2. Voltage dependence of the junctional resistance. (A) Hypothesized current flow under different conditions of junctional polarization. The GMS is opened or interrupted (heavy bar) during high or low synaptic conductance states, respectively. Only currents schematized by solid lines cross the synapse [modified from (*4*)]. (B to D) Changes of coupling variables produced during one experiment by hyperpolarization of the postsynaptic fiber. (B) Relationship between voltages recorded in the presynaptic and postsynaptic cells at different ΔV's, labeled from a to i (a = −11; b = −1; c = +20; d = +23; e = +30; f = +35; g = +43; h = +50; i = +56 mV; each curve corresponds to no less than 22 data points, which are omitted for clarity). (C) Currents of equal amplitude (I = 280 nA, equivalent to +17- or −23-mV charges) and opposite sign were applied presynaptically. As the postsynaptic fiber was made more negative, coupling coefficients for positive (solid line) and negative pulses (dashed line) gradually increased. (D) Relations between the junctional resistances and the voltage difference across the synapse. [The points of parts (C) and (D) were calculated after the same injections.]

+35 mV (mean = 39 ± 6 mV; N = 21). The 10- to 20-fold drop in the junctional membrane resistance R_J is less than predicted from indirect measures (*4*).

In order to confirm that the conductance increase depended on junctional polarization rather than on other variables, such as postsynaptic voltage alone, polarizing pulses were also applied presynaptically. As expected, the antidromic spread of hyperpolarizing currents was reduced and then suppressed by making ΔV more negative with this procedure (Fig. 3A), which, however, was limited in the opposite direction by delayed rectification. The preparation was thus perfused with a solution containing tetrodotoxin and 4-aminopyridine, which allowed the lateral axon to be depolarized by as much as 50 to 60 mV. Electrotonic coupling was then enhanced for both negative and positive currents injected in the motor axon, with depolarizing currents spreading to the presynaptic fiber as illustrated by the sample traces of Fig. 3, B_1 and B_2.

The input resistance R_I (mean equal 100 kilohm at rest) of the giant motor fiber was reduced when ΔV became positive (Fig. 3C). This finding was important because a current delivered in the giant motor fiber will also flow through three electrotonic synapses disposed in parallel (Fig. 3D), and the equations generally used to calculate R_J directly are inappropriate. Yet, these variations confirmed that concomitant modifications of the coupling coefficient ratio were mostly induced by changes of the junctional permeabilities (*1, 12*).

Similar observations of voltage-dependent coupling coefficients were collected at the rectifying connections between the motor fiber and the ipsi- or contralateral medial giant axons (Fig. 3D) where ΔV was, at rest, of the same order of magnitude as in the GMS. Unidirectional transmission may well be associated with a potential difference across the gap junctions, which is also present and of about 15 mV at rectifying synapses between giant fibers and motoneurons of the hatchetfish (*13*), in the ommatidium of limulus (*14*), and in the spinal cord of the lamprey (*15*), but information is needed about those of *Aplysia* (*16*) or leech (*17*) before generalizing. Along this line, our attempts to modify R_J at the septate junction, which is normally not polarized, were never successful.

Since the kinetics of the conductance change are so fast, ΔV was also assessed during the test pulse itself, and a comparable voltage dependency of R_J was found. On the other hand, given the location of the electrodes, the estimated polarization, no matter how defined, could only approximate the actual potential imposed across the synaptic membrane.

Voltage sensitivity at the GMS is markedly different from that between amphibian embryonic cells. In early embryos, the junctional conductance is decreased by transjunctional polarization in either direction, the kinetics of uncoupling is extremely slow, and a fraction of the conductance is insensitive to voltage variations (*7, 18*). Even this last property could not be demonstrated at the GMS: during the maximum bidirectional transmission, the coupling ratios for positive and negative currents (0.63 ± 0.10 versus 0.59 ± 0.09; N = 22) and the junctional resistances (69 ± 15 versus 97 ± 27 kilohm; N = 22) were not statistically different [Wilcoxon–Mann-Whitney tests (*19*)].

Ionic accumulation or current-dependent mechanisms could not account for the increased conductance: changes in H^+ and Ca^{2+} cytoplasmic concentrations were unlikely, since injection of these ions in either side of gap junctions does not create asymmetrical transmission (*20*) and the high conductance condition was independent of the amount of current injected to shift ΔV once a plateau was reached. Also, a simple interposition of classical voltage-sensitive membrane to junctional membrane is not supported by the observed modifications of input impedances as R_J varies. It seems that gap junctions at the GMS have either the voltage-dependence typical of many aqueous channels, the electron transfer properties of solid-state elements, or both. In this context, quantum mechanical tunneling currents have been characterized in artificial bimolecular membranes with Zener-diodic properties (*21, 22*); that such a tunneling effect takes place across polarized gaps has been suggested (*23*). Further knowledge of gap junctional molecular structure is required to reconcile these concepts. In any case, our results strengthen the notion that the permeabilities of electrotonic synapses are not necessarily controlled in the same manner, despite their apparent uniform ultrastructure.

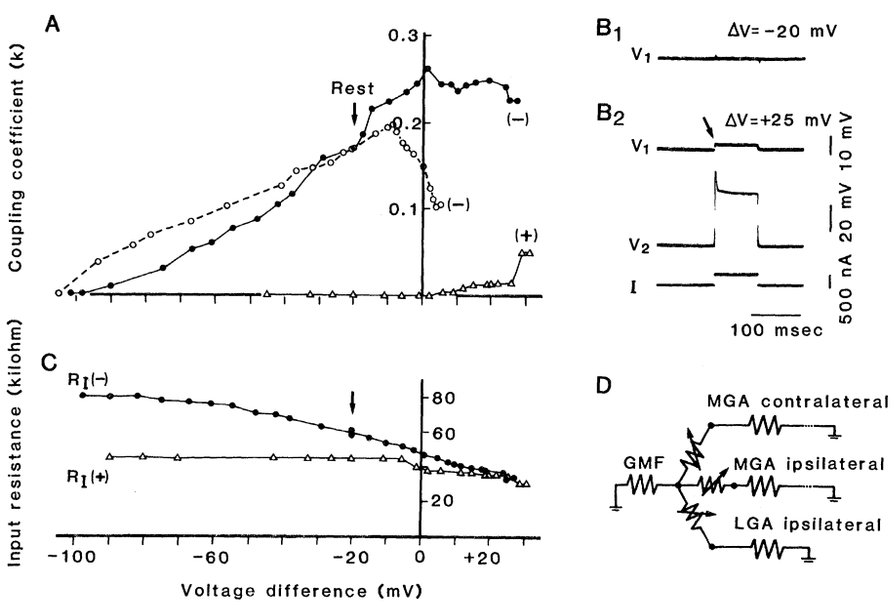

Fig. 3. Transynaptic spread of currents in the antidromic direction. (A to C) The potential difference across the GMS was modified in the presynaptic axon, and negative (−) or positive (+) pulses (I = −540 and +590 nA corresponding to +35 and −54 mV potential changes) were applied in the motor fiber. (A) Coupling coefficients as a function of ΔV in control conditions (dashed line) and in the presence of a tetrodotoxin (50 μ*M*) and 4-aminopyridine (5 m*M*) solution (solid lines). Negative (filled circles) or positive (open triangles) test pulses were used. (B_1 and B_2) Sample recordings illustrating that no voltage variation was produced at rest in the lateral axon (B_1) by a postsynaptic depolarizing current (I) which, by contrast, became adequate to generate a presynaptic response (B_2, arrow) when ΔV was shifted to +25 mV in the presence of tetrodotoxin and 4-aminopyridine. (Voltage deflection introduced by the polarizing current was omitted.) (C) Relations between the input resistance of the postsynaptic cell and ΔV in presence of tetrodotoxin and 4-aminopyridine. (D) Equivalent circuit of the electrical synapses established by the giant motor fiber. Rectifying junctions are represented as variable resistors. Abbreviations: *GMF*, giant motor fiber; *LGA*, lateral giant axon; *MGA*, medial giant axon.

CHRISTIAN GIAUME
HENRI KORN
Institut Pasteur, INSERM, Laboratoire de Neurobiologie Cellulaire, Département de Biologie Moléculaire, 25 Rue du Docteur Roux, 75015 Paris, France

References and Notes

1. M. V. L. Bennett, *Ann. N.Y. Acad. Sci.* **137**, 509 (1966).
2. _____, in *Structure and Function of Synapses*, G. D Pappas and D. P. Purpura, Eds. (Raven, New York, 1972), pp. 221–256.
3. C. A. G. Wiersma, *J. Neurophysiol.* **10**, 23 (1947).
4. E. J. Furshpan and D. D. Potter, *J. Physiol. (London)* **145**, 289 (1959).
5. J. J. Wine and F. B. Krasne, *J. Exp. Biol.* **56**, 1 (1972).
6. J. J. Robertson, *Ann. N.Y. Acad. Sci.* **94**, 339 (1961); J. S. Keeter, R. B. Hanna, G. D. Pappas, *J. Cell Biol.* **79**, 764 (1978); C. Peracchia, *Int. Rev. Cytol.* **66**, 81 (1980).
7. D. C. Spray, A. L. Harris, M. V. L. Bennett, *Science* **204**, 432 (1979).
8. A. Van Harreveld, *Proc. Soc. Exp. Biol. Med.* **34**, 428 (1936).
9. Since one current microelectrode was used to change membrane potential, the junctional membrane resistance R_j was calculated according to simplified equations derived elsewhere [Y. Asada and M. V. L. Bennett, *J. Cell Biol.* **49**, 159 (1971)].
10. R. Ochi, *Pfluegers Arch.* **311**, 131 (1969); W. J. Moody, *J. Physiol. (London)* **316**, 293 (1981).
11. E. J. Furshpan and D. D. Potter, *J. Physiol. (London)* **145**, 326 (1959).
12. W. R. Loewenstein, M. Nakas, S. J. Socolar, *J. Gen. Physiol.* **50**, 1645 (1967); B. Rose and R. Rick, *J. Membr. Biol.* **44**, 377 (1978).
13. A. A. Auerbach and M. V. L. Bennett, *J. Gen. Physiol.* **53**, 211 (1969). The junctional resistance in this preparation exhibits a voltage dependency similar to that at the GMS, but no plateau was reached in this preparation.
14. T. G. Smith and F. Baumann, *Prog. Brain Res.* **31**, 313 (1969).
15. G. L. Ringhmam, *J. Physiol. (London)* **251**, 395 (1975).
16. A. Arvanitaki and N. Chalazonitis, *Bull. Inst. Oceanogr. Fish.* **1143**, 1 (1959).
17. J. G. Nicholls and D. Purves, *J. Physiol. (London)* **209**, 647 (1970).
18. D. C. Spray, A. L. Harris, M. V. L. Bennett, *J. Gen. Physiol.* **77**, 77 (1981).
19. H. B. Mann and D. R. Whitney, *Ann. Math. Stat.* **60**, 50 (1947).
20. W. C. De Mello, *Cell Biol. Int. Rep.* **4**, 51 (1980); W. R. Loewenstein, *Physiol. Rev.* **61**, 829 (1981).
21. B. Mann and H. Kuhn, *J. Appl. Phys.* **42**, 4398 (1971); H. C. Pant and B. Rosenberg, *Biochim. Biophys. Acta* **225**, 379 (1971).
22. B. Rosenberg, *Discuss. Faraday Soc.* **51**, 190 (1971).
23. E. H. Walker, *Int. J. Quantum Chem.* **11**, 103 (1977).

24. Supported in part by INSERM grant C.R.L. 81.60.42 and DGRST grant 81.E.0576. We thank A. Aurengo for help with statistics and J. Nicolet for technical and secretarial assistance.

18 June 1982; revised 30 September 1982

Mechanical Action of the Intercostal Muscles on the Ribs

Abstract. *The external and internal interosseous intercostal muscles were separately stimulated at end-expiratory lung volume in anesthetized dogs. These muscles were all found to elevate the ribs into which they insert. By attaching weights to the ribs, it was determined that the nonlinear compliance of the ribs was responsible for this phenomenon.*

The action of the intercostal muscles has been a subject of controversy throughout medical history (*1*). Up to the middle of this century, varying and opposite points of view found strong supporters (*2*). At present, the most widely held view is that associated with Hamberger (*3*), whose theory, inferred from the anatomical relations of the muscles (points of origin and insertions), is that the external intercostals and the interchondral portion of the internal intercostals (the parasternals) elevate the ribs to which they are attached and, accordingly, are inspiratory, while the interosseous portion of the internal intercostals lowers the ribs and, therefore, is expiratory.

Electrical recordings from the intercostal muscles in normal humans showed a phasic behavior of these muscles which was in accord with Hamberger's theory (*4*). Electromyographic observations, however, cannot be interpreted correctly as long as the mechanical action of the muscles remains unknown. Motions are frequently complex, requiring contraction not only of agonists but also of synergists, fixators, and even antagonists. Electrical activity of a muscle associated with a particular motion does not prove that the muscle is the agonist. The observation that one intercostal muscle contracts during inspiration and that this contraction is associated with an enlargement of the rib cage, therefore, does not prove that the muscle is inspiratory in function (that is, causes flow of air into the lungs), nor does it prove that the action of the muscle is to raise the lower rib into which it is inserted; the ribs could be displaced by other muscles and the electrical activity observed in the intercostals might be fixating or antagonistic (*2*). With the exception of the parasternals, which were recently shown to be inspiratory (*5*), there is no direct experimental evidence that establishes the mechanical action of the intercostal muscles. In this report we show that at end-expiratory lung volume, both the external and the interosseous internal intercostals elevate the ribs into which they insert. We also show that this phenomenon results from the nonlinear compliance of the ribs.

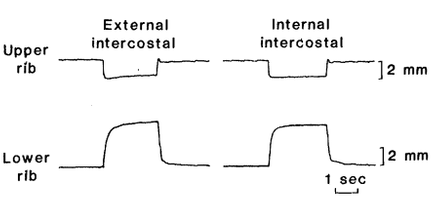

Fig. 1. Effect of stimulating separately the external and the internal interosseous intercostal muscle in one intercostal space on the axial displacements of the ribs situated immediately above (upper trace) and below (lower trace). In the two channels, upward deflections indicate a cephalad displacement, and downward deflections the reverse. In this record, the stimulation frequency was 100 Hz.

Experiments were performed on supine dogs anesthetized with sodium pentobarbital (25 mg/kg), intubated, and maintained under deep general anesthesia with supplementary doses. The rib cage and the intercostal muscles were exposed from the second to the tenth rib by deflection of the skin and the consecutive layers of muscles. Hooks were screwed into two adjacent ribs on the anterior or midaxillary line and connected by inextensible threads to linear displacement transducers positioned along the longitudinal body axis of the animal in order to measure the axial displacements of the ribs (*5*). A pair of stimulating electrodes spaced 2 cm apart was then inserted superficially in the fibers of the external intercostal muscle connecting the two ribs. The stimulus (20 to 100 Hz, 0.2 msec) was adjusted from 5 to 10 V for maximum effect without activation of the other intercostal muscles of the same interspace (*6*). After the external intercostal was studied, the muscle was removed and the internal interosseous intercostal was exposed and stimulated. All measurements were obtained at end-expiratory lung volume during apnea induced by hyperventilation. Studies were made on 28 intercostal spaces in 12 animals.

Representative records are shown in Fig. 1. Electrical stimulation of the external intercostal resulted in a cephalad displacement of the rib situated below and a caudad displacement of the rib situated above the muscle. The cephalad displacement of the lower rib was, however, twice as large as the caudad displacement of the rib above. For the ribs to which it is attached, therefore, the net effect of contraction of the external intercostal muscle was inspiratory. Stimulation of the interosseous portion of the internal intercostal also resulted in a cephalad displacement of the lower rib and a caudad displacement of the rib above. Here also, the cephalad displacement of the lower rib was about twice as large as the caudad displacement of the upper rib. The net action of the internal interosseous intercostal muscle, therefore, was also inspiratory for the ribs into which it inserts. Almost identical records were obtained for all the interspaces investigated. There was no differ-